Disruptions in endocytic traffic contribute to the activation of the NLRP3 inflammasome

DOI:
10.1126/scisignal.abm7134

Document Version
Accepted author manuscript

Citation for published version (APA):
Lee, B., Hoyle, C., Wellens, R., Green, J. P., Martin-Sanchez, F., Williams, D. M., Matchett, B. J., Seoane, P. I., Bennett, H., Adamson, A., Lopez-Castejon, G., Lowe, M., & Brough, D. (2023). Disruptions in endocytic traffic contribute to the activation of the NLRP3 inflammasome. *Science Signaling*, *16*(773). https://doi.org/10.1126/scisignal.abm7134

Published in:
Science Signaling

One-Sentence Summary: The NLRP3 inflammasome senses and is activated by perturbations in endosomal trafficking.

Editor's Summary:

Inflammation-inducing traffic jams

The NLRP3 inflammasome assembles and is activated by diverse cellular stresses to produce proinflammatory cytokines. Lee *et al.* investigated whether the NLRP3 inflammasome was activated by disruptions in endosomal trafficking. By analyzing various cell types, including bone marrow-derived macrophages, the authors found that NLRP3-activating stimuli resulted in perturbations in endosomal trafficking and conversely, that chemical interference with endosomal trafficking potentiated NLRP3 activation, although it was insufficient to activate NLRP3 by itself. Activated NLRP3 was recruited to endolysosomal vesicles, where it colocalized with the lipid PI4P, which the authors speculated may be the additional stimulus required for NLRP3 activation. Thus, NLRP3 senses and is activated by cellular stress resulting from disordered endosomal trafficking.

Title: Disruptions in endocytic traffic contribute to the activation of the NLRP3 inflammasome*

Authors: Bali Lee[1,4,5#], Christopher Hoyle[1,4,5#], Rose Wellens[1,4,5], Jack P. Green[1,4,5], Fatima Martin-Sanchez[2,5], Daniel M. Williams[1,6], Billie J. Matchett[1,4,5], Paula I. Seoane[1,4,5], Hayley Bennett[7], Antony Adamson[7], Gloria Lopez-Castejon[2,5], Martin Lowe[3*], David Brough[1,4,5*]

Affiliations:

[1]Division of Neuroscience, School of Biological Sciences, Faculty of Biology, Medicine and Health, University of Manchester, Manchester Academic Health Science Centre, Manchester, M13 9PT, UK.

[2]Division of Infection, Immunity and Respiratory Medicine, School of Biological Sciences, Faculty of Biology, Medicine and Health, Manchester Academic Health Science Centre, University of Manchester, Manchester, M13 9PT, UK.

[3]Division of Molecular and Cellular Function, School of Biological Sciences, Faculty of Biology, Medicine and Health, Manchester Academic Health Science Centre, University of Manchester, Manchester, M13 9PT, UK.

[4]Geoffrey Jefferson Brain Research Centre, The Manchester Academic Health Science Centre, Northern Care Alliance NHS Group, University of Manchester, Manchester, M13 9PT, UK.

[5]The Lydia Becker Institute of Immunology and Inflammation, University of Manchester, Manchester, M13 9PT, UK.

[6]Department of Biomedical Science, Centre for Membrane Interactions and Dynamics, University of Sheffield, Firth Court, Sheffield S10 2TN, UK.

[7]Genome Editing Unit, Faculty of Biology, Medicine and Health, University of Manchester, Manchester, M13 9PT, UK

[#]Contributed equally

*Corresponding authors. Emails: david.brough@manchester.ac.uk, martin.p.lowe@manchester.ac.uk

Abstract

Inflammation driven by the NLRP3 inflammasome is coordinated through multiple signaling pathways and is regulated by sub-cellular organelles. Here, we tested the hypothesis that NLRP3 senses disrupted endosome trafficking to trigger inflammasome formation and inflammatory cytokine secretion. NLRP3-activating stimuli disrupted endosome trafficking and triggered localization of NLRP3 to vesicles positive for endolysosomal markers and for the inositol lipid PI4P. Chemical disruption of endosome trafficking sensitized macrophages to the NLRP3 activator imiquimod, driving enhanced inflammasome activation and cytokine secretion. Together, these data suggest that NLRP3 can sense disruptions in the trafficking of endosomal cargoes, which may explain in part the spatial activation of the NLRP3 inflammasome. These data highlight mechanisms that could be exploited in the therapeutic targeting of NLRP3.

Introduction

The NLRP3 (NLR family pyrin domain containing 3) inflammasome is a multi-molecular protein complex that regulates the processing and secretion of the pro-inflammatory cytokines interleukin (IL)-1β and IL-18. NLRP3 inflammasome activation in cells of the innate immune system occurs when the cytosolic protein NLRP3 senses diverse cellular stressors and undergoes post-translational modifications and a conformational change to enable interaction with an adaptor protein called ASC (apoptosis-associated speck-like protein containing a CARD). The subsequent oligomerisation of ASC into a ‘speck’ provides a platform for the recruitment and activation of the protease caspase-1, which cleaves inactive precursors or pro-forms of IL-1β and IL-18 to facilitate their release from the cell and catalyses pyroptotic cell death (*1*). NLRP3-dependent inflammation contributes to the worsening of diverse diseases and although there are inhibitors of NLRP3 being developed (*2*), we do not fully understand the mechanisms leading to its activation. In macrophages, the activation of the canonical NLRP3 inflammasome requires two stimuli. The first is required to induce expression of the NLRP3 protein itself in a step known as priming, and experimentally this is usually achieved by treatment of cells with the pathogen-associated molecular pattern (PAMP) lipopolysaccharide (LPS), a bacterial endotoxin (*3*). To induce

assembly of an active NLRP3 inflammasome, the primed cell needs to then encounter an additional PAMP, or damage-associated molecular pattern (DAMP), or another activating stimulus. For both steps in the canonical pathway, post-translational modifications, such as ubiquitination or deubiquitination and phosphorylation or dephosphorylation of NLRP3, are required for inflammasome formation (*1*). Structurally diverse PAMPs, DAMPs, and other stimuli are reported to activate NLRP3 by altering cellular homeostasis (*4*). We reviewed literature highlighting that multiple organelle stresses are linked to NLRP3 inflammasome activation and suggested a potential role for endosomes in the process (*1*). Dispersion of the trans-Golgi marker TGN38 (TGN46 in primates) occurs after treatment of cells with NLRP3-activating stimuli (*5*). TGN38/46 does not permanently reside in the TGN and cycles through the plasma membrane and endosomes before returning to the TGN. Cycling of TGN38/46 is interrupted by modification of endosomal pH with vacuolar ATPase inhibitors or K^+ ionophores, both of which cause an accumulation of TGN38/46 in early endosomes (*6, 7*). K^+ ionophores also activate NLRP3 (*8*), and other activators of NLRP3 (such as hypo-osmotic stress, and the K^+-efflux-independent stimuli imiquimod and CL097), also perturb endosomal pH (*9, 10*). Thus, inflammasome activation may also be associated with perturbed endosome function. Moreover, endosomes provide a signalling hub for pattern recognition receptors (PRRs) such as members of the Toll-like receptor (TLR) family, identifying this organelle as a site of importance for inflammatory signalling (*11*). We therefore tested the hypothesis that NLRP3 senses and is activated by disrupted endosome trafficking.

Results

TGN38/46 trapping in endosomes

Initially we set out to test the hypothesis that NLRP3-activating stimuli cause trapping of TGN38/46 in the endosome. These NLRP3-activating stimuli included the K^+ ionophore nigericin (*12*), lysosomal disrupting agent L-leucyl-L-leucine methyl ester (LLOMe) (*13*), and imiquimod, which activates NLRP3 independently of K^+ efflux (*10*). The Na^+ ionophore monensin was included as a control because it disrupts endosome trafficking (*7*). In unstimulated COS7 cells, there was strong co-localization between TGN46 and the permanent TGN resident protein Golgin97, with both proteins localizing to the peri-nuclear TGN, as expected (Fig. 1A&B). Treatment with NLRP3-activating stimuli or monensin caused dispersal of TGN46 to cytoplasmic puncta and a reduction in the co-localization of TGN46 with Golgin97, which remained peri-nuclear (Fig. 1A&B, fig. S1A). Of the NLRP3-activating stimuli tested, imiquimod had the mildest

effect on TGN46 localization (Fig. 1B, fig. S1A), although it is reported to have diverse effects on endolysosomal organelles which could further account for its effects (*14, 15*). These data suggest that under these conditions, NLRP3-activating stimuli induced the vesicular localization of TGN46 whereas the TGN, as defined by Golgin97, remained largely intact. TGN46 becomes trapped in early endosomes when endosome-to-Golgi trafficking is perturbed (*6, 7*). Thus, we investigated whether the TGN46 puncta represented endosomes. In untreated cells, there was little co-localization between TGN46 and the early endosomal marker EEA1 (Fig. 1C&D). However, in response to the NLRP3-activating stimuli or monensin, there was a significant increase in TGN46 and EEA1 co-localization (Fig. 1C&D, fig. S1B). The NLRP3-activating stimuli and monensin also affected the distribution of CD63-positive late endosomes, which became more scattered after stimulation (Fig. 1E, fig. S1C). These scattered CD63 endosomes also co-localized with TGN46 with the exception of imiquimod treatment (Fig. 1E&F, fig. S1C). Similar to CD63, NLRP3-activating stimuli induced the colocalization of TGN46 with the lysosomal marker LAMP1, with the exception of LLOMe, which is a lysosomal disrupting agent (fig. S2A&B). There were minimal changes in co-localization with the recycling endosome marker MICAL-L1 (fig. S2C&D). These data indicate that trapping of TGN46 in endolysosomal compartments is a common outcome of treatment with NLRP3-activating stimuli. Time course experiments in COS7 (fig. S3A&B), HeLa (fig. S4A&B), and primary mouse bone marrow-derived macrophages (BMDMs)(fig. S3C&D) showed that TGN46/38 became vesicular shortly after the application of nigericin. Co-localization of TGN46/38 and Golgin97 in COS7, BMDM, and HeLa cells was significantly decreased after 30 minutes (fig. S3A-D, S4A&B), consistent with this being an early event preceding NLRP3 inflammasome activation. These results are also consistent with previously published data showing an early (5 minutes post stimulation) vesiculation of TGN38 in mouse BMDMs stimulated with ATP or nigericin (*5*). Neither COS7 nor HeLa cells used in these experiments expressed NLRP3, whereas THP1 human monocyte cells endogenously express NLRP3 (fig. S5D). Nigericin still caused TGN46 vesiculation in WT THP1 cells and to a lesser extent in THP1 cells with NLRP3 knockout (fig. S5A,B&C).

We next assessed the effects of the stimuli on TGN38 distribution in primary mouse BMDMs, cells commonly used to study NLRP3 inflammasome activation. In untreated and LPS-treated BMDMs, Golgin97 and TGN38 co-localized in the peri-nuclear TGN (Fig. 2A&B). Treatment with NLRP3-activating stimuli (except imiquimod) or monensin caused a decrease in Golgin97 and TGN38 co-localization, with a concomitant increase in TGN38 dispersion, similar to that seen

in COS7 cells (Fig. 2A&B, fig. S6A). Similar effects were observed with additional stimuli, silica crystals and ATP (fig. S7). Only treatment with the NLRP3-activating stimulus LLOMe caused significant co-localization of TGN38 with EEA1, though some co-localization was detected with the other stimuli (Fig. 2C&D, fig. S6B). In LPS-treated BMDMs, nigericin, LLOMe, and imiquimod all induced IL-1β release, which was attenuated by the NLRP3 inhibitor MCC950 (Fig. 2E). Monensin did not induce IL-1β release despite inducing dispersal of TGN38, suggesting that TGN38 dispersal alone is not sufficient for NLRP3 activation. To further test whether scattering of the TGN was sufficient for NLRP3 activation, cells were treated with nocodazole, which disrupts microtubules and induces scattering of the Golgi apparatus (*16*). As expected, treatment of LPS-primed BMDMs with nocodazole caused the Golgi to scatter throughout the cytosol but did not alter the extent of colocalization between TGN38 and Golgin97 (fig. S8A&B). Nocodazole also did not stimulate NLRP3 inflammasome activation or affect IL-1β release after nigericin treatment (fig. S8C), suggesting that scattering of the TGN per se is not sufficient for NLRP3 activation, and that the separation of TGN38/46 from Golgin97 described above was caused by a trafficking defect. We also examined the effects of nocodazole on the Golgi in GFP-NLRP3-expressing COS7 cells (*17*). In resting cells, the NLRP3 signal was predominantly localized to the TGN and the cytosol (fig. S8D). Treatment with nocodazole scattered the Golgi without affecting the colocalization of Golgin97 and NLRP3 (fig. S8D,E), reminiscent of the effect observed in macrophages.

NLRP3-activating stimuli disrupt endosomal trafficking

We next set out to directly test whether NLRP3-activating stimuli disrupt endosome-to-TGN cycling, which could account for the observed redistribution of TGN38/46 to endosomes. To assess the effects of NLRP3-activating stimuli and monensin on endosome to TGN trafficking we used fluorescently-labelled Shiga toxin B-subunit (STxB-Cy3) as described previously (*18*). STxB is internalised to early endosomes from where it undergoes retrograde transport to the TGN en route to the endoplasmic reticulum (Fig. 3A). All stimuli reduced co-localization of STxB-Cy3 and Golgin97 at 20 minutes (Fig. 3B&C, fig. S9A). At 45 minutes, there was increased co-localization with STxB-Cy3 and Golgin97 in vehicle-treated cells, which was significantly reduced after LLOMe, monensin, or nigericin treatment (Fig. 3B&C). These results indicate that endosome to TGN trafficking is impaired by NLRP3 inflammasome-activating stimuli.

We next investigated whether NLRP3-activating stimuli and monensin caused a more general disruption of endosome trafficking by looking at other endosome trafficking steps. Iron-loaded transferrin is endocytosed by clathrin-coated vesicles into early endosomes, where it releases bound iron due to the acidic luminal pH, before recycling back to the plasma membrane, either directly or through recycling endosomes, to the extracellular space (*19, 20*) (Fig. 3D). Using a modified version of a previously described assay that measures transferrin uptake, endocytosis, and recycling (*21*), we found that none of the NLRP3-activating stimuli tested or monensin reduced transferrin uptake, except for nigericin which had a small effect. In contrast, all treatments caused retention of transferrin within cells (Fig. 3E&F, fig. S9B&C). This effect on transferrin recycling was most apparent for nigericin and monensin, although all stimuli caused decreased cycling (Fig. 3E&F), indicating that endosomal recycling to the plasma membrane was perturbed by all NLRP3-activating stimuli tested, as well as monensin.

We next investigated the effects of NLRP3-activating stimuli on trafficking from endosomes to lysosomes with an epidermal growth factor (EGF) trafficking assay (*21, 22*) (Fig 3G). Intracellular EGF fluorescence assayed 1 and 2 hours post-stimulation by fluorescence microscopy showed that all treatments significantly prevented the degradation of EGF, suggesting that they had prevented trafficking to lysosomes (Fig. 3H&I, fig. S9D). These data show that the NLRP3-activating stimuli nigericin, LLOMe, and imiquimod perturb endosomal trafficking pathways with imiquimod having the mildest effect of stimuli tested. Thus, all NLRP3-activating stimuli investigated perturbed endosome trafficking to some extent.

Effects of perturbing endosomal trafficking on NLRP3 activation

The data so far indicated that NLRP3-activating stimuli disrupt endosomal trafficking. The inability of monensin to activate NLRP3 despite its ability to disrupt endosome cycling suggests that perturbed endosomal trafficking may contribute to NLRP3 inflammasome activation but is by itself insufficient. We hypothesised that the effects of NLRP3-activating stimuli could be potentiated by disrupting endosome trafficking. Because imiquimod caused the mildest perturbation of endosomal trafficking of the NLRP3-activating stimuli tested, we sought to potentiate the effects of imiquimod by perturbing endosome trafficking with monensin. Monensin pre-treatment of LPS-primed BMDMs significantly potentiated imiquimod-induced IL-1β release and cell death (Fig. 4A&B), ASC oligomerisation (measured as described previously (*23*)) (Fig. 4C), and processing of caspase-1 and gasdermin D (Fig. 4D). Monensin treatment alone did not

induce IL-1β release (Fig. 4A). The exacerbation of IL-1β release and cell death caused by monensin pre-treatment were NLRP3-dependent because they were blocked by the specific NLRP3 inhibitor MCC950 (Fig. 4E&F). We further explored the effects of monensin pre-treatment on ASC speck formation. In WT immortalized mouse BMDMs (iBMDMs), monensin enhanced imiquimod-dependent IL-1β release and cell death (Fig. 4G&H), and in iBMDMs stably expressing ASC labelled with the fluorescent protein mCherry (*24*), it significantly enhanced NLRP3-dependent ASC oligomerization and speck formation (Fig. 4I-M). This increase in ASC speck formation was due to more cells forming ASC specks, rather than multiple specks forming in the same cells (Fig. 4K&L). In the absence of imiquimod, monensin did not affect IL-1β release or ASC speck formation in LPS-treated cells. We also examined the effects of these treatments on Golgin97 and TGN38 colocalization and distribution in LPS-primed iBMDMs. In vehicle-treated cells, both Golgin97 and TGN38 were colocalized in the peri-nuclear region (fig. S10A&B). Monensin treatment reduced the degree of co-localization of Golgin97 and TGN38, consistent with effects on endosome to TGN cycling (fig. S10A&B). Imiquimod had minimal effects on Golgin97 and TGN38 distribution, whereas in imiquimod-treated cells that had undergone prior treatment with monensin, Golgin97 and TGN38 colocalization was reduced (fig. S10A&B).

To further investigate this effect, we analysed how varying the dose of imiquimod influenced the response and compared this to nigericin (fig. S11A-D). Monensin potentiated the effects of imiquimod on inflammasome activation even at sub-threshold concentrations of imiquimod (fig. S11C&D). However, monensin did not significantly affect nigericin-induced IL-1β release or cell death (fig. S11A&B). Given that nigericin and monensin are both ionophores, there could be confounding effects complicating the interpretation of these data. A related study showed that knocking out proteins involved in endosome-to-TGN retrograde trafficking such as ADP ribosylation factor related protein 1 (ARFRP1) and SYS1 in THP1 cells enhanced NLRP3 inflammasome activation. It was also reported that the endosome to TGN retrograde trafficking inhibitor Retro-2 (*25*) enhances NLRP3 inflammasome activation in THP1 cells (*26*). We therefore tested whether Retro-2 could potentiate NLRP3 inflammasome activation in our experiments as further evidence of disrupted endosome trafficking contributing to inflammasome activation. Retro-2 had a small but significant effect on imiquimod-induced NLRP3 activation in primary BMDMs (fig. S12A&B), and significantly potentiated NLRP3 activation in immortalized BMDMs (fig. S12C-I). Accepting the caveats of these experiments, these data suggest that disrupting endosome trafficking can potentiate NLRP3 inflammasome activation.

NLRP3 can localize to membranes of endolysosomal origin

Because our results suggested a link between dysregulation of endosomal trafficking and NLRP3 stimulation, we next wanted to assess whether NLRP3 could localize to endolysosomal membranes in stimulated cells. In unstimulated COS7 cells stably expressing low levels of NLRP3-mVenus, NLRP3-mVenus was localized predominantly in the cytosol and peri-nuclear TGN (Fig. 5A-C, fig. S13). Stimulation with NLRP3-activating stimuli or monensin caused a redistribution of some of the NLRP3-mVenus to cytoplasmic puncta that partially co-localized with EEA1- and CD63-containing endosomes as well as LAMP1-containing lysosomes (Fig. 5A-C, fig. S14A-C, S15A-D). In contrast, NLRP3-mVenus puncta rarely co-localized with the trans-Golgi marker Golgin97 after stimulation (fig. S13, S15A). These data suggest that NLRP3 can localize to multiple endolysosomal membranes upon stimulation, consistent with a previous report of co-localization of TGN38, EEA1, and NLRP3-GFP in nigericin-treated HeLa cells (*5*). Furthermore, as presented in a related study, activated NLRP3 localizes to RAB5-positive endosomes after stimulation (*26*). NLRP3 associates with the inositol lipid PI4P (*5*) and other phosphatidylinositides (*27*). To ascertain whether NLRP3 localizes to PI4P-containing membranes upon stimulation, we transiently transfected the PI4P probe SidM-mCherry (*28*) into NLRP3-mVenus-expressing COS7 cells. Under resting conditions, NLRP3 was generally diffuse in the cytosol, whereas the PI4P probe concentrated on the TGN, as expected (*28*) (Fig. 6A, fig. S17A). Upon treatment with nigericin or LLOMe, PI4P accumulated on discrete cytoplasmic puncta, many of which co-localized with NLRP3 (Fig. 6A&B, and fig. S16A&B). Monensin did induce a small reduction in colocalization between the PI4P probe and Golgin97 (Fig. 6C). However, monensin did not appear to cause a redistribution of the PI4P probe to cytoplasmic puncta, but did cause NLRP3 to localise to puncta as expected (Fig. 6A&D). In response to NLRP3-activating stimuli, the PI4P-containing puncta partially colocalized with markers of late endosomes (Fig. 6D&E, fig. S16D&E) and of lysosomes (Fig. 6F&G, fig. S16F&G). The failure of monensin to impact PI4P distribution could partially explain why it is not a sufficient stimulus for NLRP3 activation, despite being able to disrupt TGN46 trafficking. Imiquimod treatment alone caused a loss of colocalization between PI4P and Golgin97 (fig. S16A&C). Imiquimod and monensin treatment together stimulated the colocalization of the PI4P probe with NLRP3 (fig. S16A&B) and between the PI4P probe and LAMP1 (fig. S16F&G). Co-localization of PI4P with EEA1 after stimulation with NLRP3 activators was limited and only observed with nigericin (fig. S17A&B).

Discussion

Organelle stress has been repeatedly linked to the activation of the NLRP3 inflammasome. We hypothesized that a cellular stress arising from disrupted endosomal cycling could serve as a trigger for NLRP3-inflammasome activation (*1*). Here, we established that NLRP3-activating stimuli caused TGN38/46 to become trapped in endosomes, which may account for at least a portion of the dispersed TGN38/46 previously observed (*5*). Further, using assays of endosome trafficking to the TGN, to the lysosomes, or to the plasma membrane (*21*), we established that all NLRP3-activating stimuli tested disrupted an aspect of endosome trafficking to some extent. These results suggested that a common effect of NLRP3-activating stimuli was disruption of endosomal trafficking. Disrupted endosomal trafficking of TGN38/46 itself, however, appeared insufficient to activate the NLRP3 inflammasome. By itself, monensin, a potent disruptor of endosome trafficking (*7*), had minimal effects on NLRP3 inflammasome activation, even at a concentration that affected endosomal trafficking of TGN38/46. These data suggest that if disruption of endosomal trafficking is important, it must occur concomitantly with another stimulation that activates NLRP3. A possible candidate is the accumulation of PI4P on endosomal and lysosomal membranes, given that NLRP3-activating stimuli but not monensin cause this effect (Fig. 7, A to C).

We included the NLRP3 inflammasome-activating stimulus imiquimod because its activation of NLRP3 occurs in the absence of K^+ ion efflux, in contrast to the majority of canonical NLRP3-activating stimuli (*10*). In all assays for endosomal trafficking investigated, imiquimod had the mildest effect, despite its ability to trap TGN46 in endosomes. When we fully disrupted endosomal trafficking by treating LPS-primed macrophages with monensin before imiquimod, NLRP3-inflammasome activation and IL-1β release were potentiated. These data highlight how manipulation of a potential endosome stress-sensing pathway interacts with an aspect of NLRP3 activation mechanisms to maximise an inflammatory response. That monensin did not potentiate nigericin-induced IL-1β release may reflect an already efficient disruption of endosome trafficking by nigericin.

Although not yet fully understood, an association of NLRP3 with membranes appears to be important for NLRP3 inflammasome activation with colocalization to TGN38/46 positive compartments observed (*5*). Furthermore, a double-ring cage of NLRP3 is proposed to represent the membrane-associated form (*27*). In addition to the work presented here, there is evidence to

suggest that NLRP3 could be recruited to endosomal membranes. For example, NLRP3 co-localizes to endosomes with complement membrane attack complexes (*29*). In macrophages, caspase-1 cleaves EEA1, and active caspase-1 co-localizes to EEA1-positive endosomes in cells treated with hypotonicity, a NLRP3-activating stimulus (*30*). Furthermore, NLRP3 can interact with PI4P through a conserved polybasic motif (*5*), and endosomal membranes contain this lipid (*28*). A related study reports NLRP3 recruitment to PI4P containing endosomes (*26*). PI4P seems likely to be important for NLRP3 membrane recruitment but may not be the only factor. For example, glycogen synthase kinase 3β (GSK3β) is reported to bind to NLRP3 and is important for its recruitment to organelle membranes (*31*). In our experiments, PI4P accumulated on CD63-positive late endosomes and LAMP1-positive lysosomes in response to NLRP3-activating stimuli. PI4P on CD63- and LAMP1-positive compartments also co-localized with NLRP3. However, monensin alone did not alter PI4P distribution, despite inducing the formation of NLRP3 puncta. Imiquimod had the mildest effect upon PI4P distribution, but when combined with monensin, induced redistribution of PI4P and NLRP3 in a manner similar to that induced by other NLRP3-activating stimuli. It is likely that NLRP3 recruitment to and concentration at endolysosomal membranes is important for its activation. However, it cannot be sufficient because monensin alone fails to activate NLRP3. Our results suggest PI4P accumulation on endolysosomal membranes may be important in the activation process, but additional events such as post-translational modification of NLRP3, which could also occur on membranes, may also be necessary. Many signalling processes occur on endosomal membranes (*11*), and inflammasome signalling may represent yet another. Whether NLRP3 persists on membranes following its activation, or dissociates, is the subject of future research. Thus, our data and other previously published observations support the possibility that NLRP3 senses disruptions to endosome trafficking, which is accompanied by accumulation of PI4P and NLRP3 recruitment onto membranes of endolysosomal origin that are important for activation of the NLRP3 inflammasome.

Understanding the activation of the NLRP3 inflammasome remains an enduring question in the field. Our data consolidate previously published observations that disruption of endosomal trafficking could likely contribute to the stress sensed by NLRP3 that is important for its activation, and that endolysosomal membranes are sub-cellular sites of importance in inflammasome activation. Further investigation into these mechanisms will reveal new insights into NLRP3 biology that may identify new ways of targeting NLRP3-dependent inflammation in disease.

Materials and Methods

Reagents

Transferrin from Human Serum, Alexa Fluor™ 488 Conjugate (T13342) and epidermal growth factor (EGF) Alexa Fluor™ 488 (E13345) were from Thermo-Fisher. Human holo-transferrin (T4132) was from Sigma-Aldrich. Shiga Toxin B-Cy3 was kindly provided by Prof. Ludger Johannes (Curie Institute, Paris). Lipopolysaccharide (LPS, *Escherichia coli 026:B*6), nigericin (N7143), ATP (A2383) and MCC950 (PZ0280) were purchased from Sigma. L-Leucyl-L-Leucine methyl ester (LLOMe, CAY16008-1) and retro-2 (CAY21946) were from Cayman Chemical, imiquimod (R837) from InvivoGen, and monensin sodium salt (5223/500) and nocodazole (1228/10) from Tocris Bioscience. Ac-YVAD-CMK (4018838) was from Cambridge Bioscience. Silica (MIN-U-SIL 15) was from U.S. Silica.

Specific antibodies were used for immunocytochemistry targeting TGN38 (0.1 μg mL^{-1}, AHP499G, Bio-Rad), TGN46 (0.25 μg mL^{-1}, AHP500GT, Bio-Rad), Golgin97 (2 μg mL^{-1}, ab84340, abcam), EEA1 (2.5 μg mL^{-1}, 610457, BD biosciences; 1:100 dilution of stock, MA5-14794, ThermoFisher), CD63 (1 μg mL^{-1}, CBL553, Sigma-Aldrich), LAMP1 (1:300 dilution of stock, MA1-164, Thermo-Fisher, or 9091, CST) and MICAL-L1 (1:100 dilution of stock, H00085377-B01P, abnova). Alexa Fluor secondary antibodies (488, 594, and 647) were from Thermo-Fisher. For Western blotting, goat anti-mouse IL-1β (AF-401-NA) was from R&D Systems, rabbit anti-mouse ASC (67824) was from CST, rabbit anti-mouse caspase-1 (ab179515) and rabbit anti-mouse gasdermin D (ab209845) were from Abcam, and rabbit anti-goat IgG (P044901-2) and goat anti-rabbit IgG (P044801-2) were from Agilent. Anti-β-actin-peroxidase (A3854) was from Sigma.

Cell Culture

HeLa and COS7 (ATCC) cells were cultured in T75 flasks in DMEM supplemented with 10% FBS, 100 U mL^{-1} penicillin, 100 μg mL^{-1} streptomycin, and 1 mM sodium pyruvate. Cells were seeded on coverslips in a 24 well plate (Corning) at 1 x 10^5 mL^{-1} density and left to adhere overnight at 37 °C and 5% CO_2. Mouse iBMDMs were originally a gift from Professor Clare Bryant (Department of Veterinary Medicine, University of Cambridge) and were modified to express ASC-mCherry in Manchester *(24)*. WT and ASC-mCherry iBMDMs were cultured in DMEM supplemented with 10% FBS, 100 U mL^{-1} penicillin, 100 μg mL^{-1} streptomycin and 1 mM sodium pyruvate, seeded at a density of 7.5 x 10^5 mL^{-1}, and left to adhere overnight at 37 °C and

5% CO_2. Primary mouse BMDMs were prepared from the femurs of 3–6 month-old WT male and female C57BL/6 mice. All procedures were performed with appropriate personal and project licenses in place, in accordance with the Home Office (Animals) Scientific Procedures Act (1986) and approved by the Home Office and the local Animal Ethical Review Group, University of Manchester. Bone marrow was harvested, red blood cells were lysed and the resulting cells were passed through a cell strainer and cultured in 70% DMEM (containing 10% FBS, 100 U mL^{-1} penicillin, 100 μg mL^{-1} streptomycin, and 1 mM sodium pyruvate), supplemented with 30% L929 mouse fibroblast-conditioned medium for 7 days at 37 °C and 5% CO_2. Cells were seeded at a density of 1 x 10^6 mL^{-1} and left to adhere overnight. Human wild-type (WT) and NLRP3 KO THP1 cells were cultured in RPMI-1640 medium supplemented with 10% (vol/vol) FBS, 100 U mL^{-1} penicillin and 100 μg mL^{-1} streptomycin and 2 mM L-glutamine. For THP1 cell stimulation, suspension cells were counted and suspended in serum-free RPMI-1640. To allow THP1 cells to adhere to coverslips for immunocytochemistry, THP1 suspension monocytes were seeded at 1 x 10^6 mL^{-1} on coverslips in a 24 well plate in the presence of PMA (250 nM for 18 h). The NLRP3 KO THP1 cells were a gift from Prof. Veit Hornung (Ludwig Maximilian University, Munich). Lenti-X 293T cells (#632180, Takara) were cultured in DMEM supplemented with 10% FBS, 100 U mL^{-1} penicillin, 100 μg mL^{-1} streptomycin and 1 mM sodium pyruvate.

Plasmids

A 3rd generation lentiviral EF1a-NLRP3-mVenus expression vector was generated by HiFi assembly (NEB). Briefly, a custom built Lenti-EF1a-Multiple cloning site-pGK-Puro vector was digested with KpnI and NotI (NEB) and column purified (Bioline). Hifi assembly fragments were amplified with HF KOD polymerase from NLRP3 (fragments 1 and 2) or mVenus (fragment 3) template DNA using the primers actagtccagtgtggtggtaccggtggatccgccaccatgaagatggcaagcacccg and tcgtcaaaggcaccttgcagctcatcgaagccgtccatgag (for fragment 1), tcatggacggcttcgatgagctgcaaggtgcctttgacg and gcagcggagccagcggagccccaagaaggctcaaagacgacg (for fragment 2), and tcgtctttgagccttcttggggctccgctggctcc and aacagatggctggcaactagaaggcacaggcggccgctcacttgtacagctcgtccatgc (for fragment 3) and assembled into the backbone vector according to the manufacturer's instructions. Vectors were transformed into NEB C3040 cells. Clones were sequenced verified. Vectors generated in this study will be submitted to Addgene. Packaging plasmids pMD2.G and psPAX2 for lentivirus production were

a gift from Didier Trono (Addgene plasmid#12259 and #12260). The GFP-NLRP3 plasmid was as described previously (*17*).

Virus production and generation of COS7 cells stably expressing NLRP3-mVenus.

Lenti-X 293 cells were plated (1 x 10^6 per well in a six-well plate) and 24h after, were transfected with 1.2 μg pMD2.G, 0.4 μg psPAX2 and 1.5 μg of NLRP3-Venus using Lipofectamine 2000 (Invitrogen). Transfection was performed following the manufacturer's instructions. 24h after transfection, the media was replaced by fresh media and cells were further incubated for 2 days. Supernatants were collected and filtered with a 0.45μm filter to obtain cell free extracts of viral particles, which were used to transduce COS7 cells. For the transduction, 5x10^4 COS7 cells plated the day before were incubated for 7h with a mix of 8 μg mL^{-1} polybrene (Sigma) and the viral particles. After 48h virus, containing media was removed and positive expressing cells were selected with puromycin 1.5 μg mL^{-1} for 10 days. Cells were FAC sorted to select a cell population homogeneously expressing NLRP3-Venus.

Transient Transfection

The day before transfection, COS7 cells, or COS7 cells stably expressing NLRP3-mVenus were seeded at 7x10^4 cells ml^{-1} in a 24-well flat-bottomed plate (Corning) and left to adhere overnight at 37°C with 5% CO_2. Cells were transfected using the Lipofectamine 3000 kit (Invitrogen) according to the manufacturer's instructions. Cells were transfected with either 100 ng of GFP-NLRP3 or 300 ng SidM-mCherry. Cell media was replaced with Opti-MEM (Thermo-Fisher), and DNA-lipid complex was added to cells and left to incubate for 20-22 hours at 37°C, 5% CO_2.

Cell stimulation

For stimulation of COS7 and HeLa cells, culture media was replaced with fresh serum-free DMEM before cells were stimulated with vehicle (ethanol 0.5% v/v), nigericin (10 μM), LLOMe (1 mM), imiquimod (75 μM) or monensin (10 μM) for 90 min, or nocodazole (10 μM) for 60 min. For stimulation of primary BMDMs, cells were first primed with either vehicle or LPS (1 μg mL^{-1}) for 4 h. The culture media was replaced with fresh serum-free media with or without MCC950 (10 μM). After 15 min cells, were stimulated with vehicle (ethanol 0.5% v/v), nigericin (10 μM), LLOMe (1 mM), imiquimod (75 μM) or monensin (10 μM) for 90 min.

For time-course experiments, COS7 and HeLa cells were seeded at a density of 1 x 10^5 mL^{-1} onto 13 mm glass coverslips and incubated in culture media overnight. Cells were stimulated with nigericin (10 μM) or vehicle (ethanol 0.5% v/v) in serum-free DMEM for 0, 10, 30 or 60 minutes. At the appropriate endpoint, cells were placed on ice, washed 3 times with sterile PBS and prepared for immunocytochemistry. Primary BMDMs were seeded at a density of 1 x 10^6 mL^{-1} onto 13 mm glass coverslips and incubated in culture media overnight. The following day, cells were primed with LPS (1 μg mL^{-1}) for 4 h. The culture media was replaced with fresh serum-free DMEM and the cells pre-treated with MCC950 (10 μM) for 15 minutes. Nigericin (10 μM) or vehicle (ethanol 0.5% v/v) was added to the wells for 0, 10, 30 or 60 minutes. At the appropriate endpoint, cells were placed on ice, washed 3 times with sterile PBS and prepared for immunocytochemistry.

For NLRP3 potentiation experiments, macrophages were primed with LPS (1 μg mL^{-1}) for 4 h (primary BMDM) or 2 h (iBMDM) before treatment with either vehicle (ethanol or DMSO 0.5% v/v), monensin (10 μM) or retro-2 (25 μM) for 1 or 2 h in serum-free DMEM. In some experiments, MCC950 (10 μM) was added for 15 min. Imiquimod (0.75-75 μM, 2 h) or nigericin (0.1-10 μM, 1 h) was added to activate NLRP3. Supernatants were collected for further analysis, or cells were prepared for Western blotting or immunocytochemistry.

Endosome trafficking assays

To evaluate Shiga toxin trafficking, HeLa cells seeded at a density of 0.25 x 10^6 mL^{-1} on 13 mm glass coverslips the day before experiments. Cells were incubated in serum free DMEM with NLRP3-activating stimuli (nigericin 10 μM, LLOMe 1 mM, imiquimod 75 μM), monensin (10 μM), or vehicle (ethanol, 0.5% v/v) for 30 min at 37°C. Cells were washed once with ice cold PBS before being incubated with Shiga toxin B-Cy3 (0.4 μg mL^{-1} in 2 mg mL^{-1} BSA in PBS) on ice for 30 min. Cells were washed twice in ice cold PBS and either fixed with PFA (4% w/v) (for a 0 min time point) or incubated in serum free DMEM with NLRP3-activating stimuli for a further 20 or 45 min at 37°C before PFA fixation. Fixed HeLa cells were incubated overnight at 4°C with specific antibodies targeting Golgin97.

To evaluate transferrin trafficking, HeLa cells were washed three times in serum free DMEM and incubated for 30 min in DMEM containing transferrin Alexa Fluor-488 (5 μg mL^{-1}) and NLRP3-

activating stimuli (nigericin 10 μM, LLOMe 1 mM, imiquimod 75 μM), monensin (10 μM) or vehicle (ethanol, 0.5% v/v). Cells underwent a 3 min ice cold acid wash (50 mM glycine, 0.1 M NaCl in dH20, pH=3) before being washed three times in serum free media containing holo-transferrin (0.1 mg mL^{-1}). Cells were either fixed (0 min) or incubated in serum free DMEM containing unlabelled holo-transferrin (0.1 mg mL^{-1}) for 15 or 30 min at 37 ºC before fixation. Cells were fixed on coverslips in 4% paraformaldehyde (PFA).

To evaluate EGF trafficking, HeLa cells were washed three times with PBS before being incubated with EGF Alexa Fluor-488 (0.4 μg mL^{-1}) in serum free DMEM (supplemented with 2% w/v BSA) on ice for 1 h. Cells were washed twice with cold PBS to remove unbound EGF-488. Cells were either fixed with 4% PFA (at the 0 min time point) or stimulated with either vehicle (ethanol 0.5% v/v), nigericin (10 μM), LLOMe (1 mM), imiquimod (75 μM), or monensin (10 μM) in serum free DMEM at 37ºC for 1 or 2 h before fixation (4% PFA).

Immunocytochemistry

Cells were fixed with 4% PFA for 20 min before being permeabilized with PBST (0.1% Triton X-100) for 5 min at room temperature. To reduce nonspecific binding of antibodies, coverslips were incubated with blocking solution (5% BSA in PBST) for 30 min at room temperature before being incubated sequentially with primary antibodies diluted in blocking solution and Alexa Fluor secondary antibodies. Nuclei were stained with DAPI. Coverslips were mounted on microslides using ProLong Gold antifade mounting reagent (Invitrogen) and left to dry overnight at room temperature.

Fluorescence microscopy and image analysis

Widefield fluorescence microscopy was used in endosomal trafficking assays using STxB-Cy3, transferrin-488 and EGF-488. Images were captured on a Zeiss Axioimager D2 upright microscope using a 63× / 1.4 Plan Apochromat objective with a Coolsnap HQ2 camera (Photometrics) and Micromanager software (v1.4.23). Specific band pass filter sets were used to prevent bleed through from one channel to the next. Images were taken of at least 3 independent fields of view per treatment per time point within each independent experiment.

1024 x 1024 pixel images were captured using a 63× / 1.40 HCS PL Apo objective on a Leica TCS SP8 AOBS inverted or upright confocal microscope with LAS X software (v3.5.1.18803). The blue diode with 405 nm and the white light laser with 488 nm, 514 nm, 594 nm and 647 nm laser lines were used, with hybrid and photon-multiplying tube detectors with detection mirror settings set accordingly. To prevent crosstalk between channels, images were acquired sequentially. Z-stacks were acquired with 0.3 µm steps between Z sections. Camera gain and exposure times were unchanged within each replicate. Images were taken from 3 independent fields of view per treatment per time point within each replicate.

Image analysis was carried out using Fiji (Image J) software. The Pearson's correlation co-efficient (PCC) for each condition was calculated using the Coloc 2 plugin. Maximum intensity projections were used for confocal images. For PCC analysis of STxB, PCC at 20 and 45 minutes was normalised against the PCC at 0 minutes for each respective stimulus to determine the change in PCC over time. For fluorescence analysis of transferrin-488 and EGF-488 trafficking, the fluorescence intensity of 7-10 cells per field of view, with 3 random fields of view analysed per experiment was measured. Background was manually calculated by taking independent measurements within each image from areas where cells were absent. The averaged background value was then subtracted from its respective mean fluorescence read-out. For transferrin-488, mean cell fluorescence was converted into percentage change against 0 minutes for each stimulus. Fluorescence intensity line graphs were created using Image J software. Fluorescence intensity of each channel was plotted individually over a 10 µm line then combined for comparison between channels. Line graphs depict fluorescence intensity between 0 and 250 grey value (a.u).

ELISA

IL-1β content in supernatants was measured by enzyme-linked immunosorbent assay (ELISA; DY401, DuoSet, R&D systems) according to the manufacturer's instructions.

LDH release assay

Cell death was determined by measuring LDH release into the supernatant using a CytoTox 96 Non-Radioactive Cytotoxicity Assay (G1780, Promega) according to the manufacturer's instructions.

ASC speck formation live imaging

iBMDMs stably expressing ASC-mCherry *(24)* were seeded overnight at a density of 7.5 x 10^5 mL^{-1} in black-walled 96-well plates. Cells were primed with LPS (1 µg mL^{-1}) for 2 h before treatment with either vehicle (ethanol 0.5% v/v) or monensin (10 µM) for 2 h in Opti-MEM. Ac-YVAD-CMK (100 µM) was added to wells with or without MCC950 (10 µM) for 15 min. Imiquimod (75 µM) or nigericin (10 µM) was added and image acquisition began immediately. Fluorescent images were acquired for 2 fields of view every 10 min for 2 h using an IncuCyte S3 Live-Cell Analysis system (Essen Bioscience) at 37 °C using a 20×/0.61 S Plan Fluor objective and the red filter set for fluorescent images. Speck numbers were quantified manually using Fiji (ImageJ).

ASC oligomerisation assay

Primary BMDMs were seeded overnight at a density of 1 x 10^6 mL^{-1} in 12-well plates. Cells were primed with LPS (1 µg mL^{-1}) for 4 h before treatment with either vehicle (ethanol 0.5% v/v) or monensin (10 µM) for 2 h in serum-free DMEM. Imiquimod (75 µM, 2 h) was added and cells were lysed in-well by direct addition of protease inhibitor cocktail and Triton-X-100 (1% v/v) into the culture medium. The combined cell lysate and supernatant was centrifuged at 6800 *x g* for 20 min at 4°C to generate Triton-X-100 soluble and insoluble fractions, which was followed by disuccinimidyl suberate (DSS)-crosslinking (2 mM, 30 min) of the insoluble fraction at room temperature as described previously *(23)*. The insoluble fraction was centrifuged at 6800 x g for 20 min at 4°C and resuspended in 1X Laemmli buffer and heated at 95°C. The Triton-X-100 soluble fraction was concentrated by adding tricholoracetic acid (10% w/v), centrifuging at 18600 *x g* for 10 min at 4°C, washing the pellet with acetone, and centrifuging again at 18600 *x g* for 10 min at 4°C. Pellets were resuspended in 2X Laemmli buffer and heated at 95°C.

Western blot analysis

BMDMs were lysed in-well by direct addition of protease inhibitor cocktail and Triton-X-100 (1% v/v) into the culture medium at the end of the experiment. The combined cell lysate and supernatant was concentrated using tricholoracetic acid precipitation as described above. Equal volumes of concentrated in-well lysates were run on 12% or 15% SDS-polyacrylamide gels and transferred at 25 V onto nitrocellulose or PVDF membranes using a Trans-Blot® Turbo Transfer™ System (Bio-Rad). Membranes were blocked in milk (5% w/v) or BSA (2.5% w/v) in PBS Tween (0.1% v/v) for 1 h at room temperature. Membranes were incubated at 4°C overnight with goat anti-mouse

IL-1β (0.25 μg mL^{-1}), rabbit anti-mouse ASC (0.101 μg mL^{-1}), rabbit anti-mouse caspase-1 (1.87 μg mL^{-1}), rabbit anti-mouse gasdermin D (0.6 μg mL^{-1}) primary antibodies in 0.1% (IL-1β), or 2.5% (ASC, caspase-1, gasdermin D) BSA in PBS Tween. The membranes were washed with PBS Tween and incubated with rabbit anti-goat IgG (500 ng mL^{-1}, 5% milk in PBS Tween) or goat anti-rabbit IgG (250 ng mL^{-1}, 2.5% BSA in PBS Tween) at room temperature for 1 h. Proteins were visualized with Cytiva Amersham ECL Prime Western Blotting Detection Reagent (GE Healthcare, RPN2236) and G:BOX (Syngene) and Genesys software. β-Actin was used as a loading control.

To detect NLRP3 in cell lysates of THP1 monocytes, HeLa and COS7 cells, supernatants were removed and cells lysed in well with lysis buffer containing Tris/HCl (50mM), NaCl (150mM), Triton X-100 (1%, v/v) and protease inhibitor cocktail (1%. v/v). Equal volumes of cell lysate were run on 10% SDS-polyacrylamide gel and transferred a 25V onto PVDF membranes using a Trans-Blot® Turbo Transfer™ System (Bio-Rad). Membranes were blocked in BSA (5% w/v) in PBS Tween (0.1% v/v) for 1h at room temperature. Membranes were incubated at 4°C overnight with mouse anti-human NLRP3 pyrin domain (1 μg mL^{-1}; Adipogen, G-20B-0014-C100) or goat anti-human NLRP3 C-terminal (0.5 μg mL^{-1}; ab4207) primary antibodies in 1% BSA in PBS Tween. The membranes were washed with PBS Tween and incubated with rabbit anti-mouse (1.3 μg mL^{-1} 1% BSA in PBS Tween) or rabbit anti-goat IgG (500 ng mL^{-1}, 1% BSA in PBS Tween) at room temperature for 1h. Proteins were visualized as described above.

Data presentation and analysis

Pearson's correlation coefficient and fluorescence intensity data are presented as median ± interquartile range (IQR) with individual data points shown (representing all cells or fields of view analyzed from each independent experiment). ELISA, ASC speck, and cell death data are presented as mean ± standard error of the mean (SEM) with individual data points shown from each independent experiment. Data were assessed for normal distribution using the Shapiro-Wilk normality test and analyzed using unpaired two-tailed t test, or one-way analysis of variance (ANOVA) followed by Dunnett's multiple comparison test, for parametric data. For non-parametric data an unpaired two-tailed Mann-Whitney test, or Kruskal-Wallis test followed by Dunn's multiple comparison test were used. Data normalized as a percentage were analyzed using multiple Mann-Whitney tests versus a value of 100%, followed by Holm-Sidak correction.

Analyses were performed using GraphPad Prism (v8). Blots are representative of 3-4 independent experiments.

Supplementary Materials

Figs. S1-17.

References and Notes

1. P. I. Seoane *et al.*, The NLRP3-inflammasome as a sensor of organelle dysfunction. *J Cell Biol* **219**, e202006194 (2020).
2. M. S. J. Mangan *et al.*, Targeting the NLRP3 inflammasome in inflammatory diseases. *Nat Rev Drug Discov* **17**, 688 (2018).
3. V. Hornung, E. Latz, Critical functions of priming and lysosomal damage for NLRP3 activation. *Eur J Immunol* **40**, 620-623 (2010).
4. A. Liston, S. L. Masters, Homeostasis-altering molecular processes as mechanisms of inflammasome activation. *Nat Rev Immunol* **17**, 208-214 (2017).
5. J. Chen, Z. J. Chen, PtdIns4P on dispersed trans-Golgi network mediates NLRP3 inflammasome activation. *Nature* **564**, 71-76 (2018).
6. B. Reaves, G. Banting, Vacuolar ATPase inactivation blocks recycling to the trans-Golgi network from the plasma membrane. *FEBS Lett* **345**, 61-66 (1994).
7. R. E. Chapman, S. Munro, Retrieval of TGN proteins from the cell surface requires endosomal acidification. *EMBO J* **13**, 2305-2312 (1994).
8. R. Munoz-Planillo *et al.*, K(+) efflux is the common trigger of NLRP3 inflammasome activation by bacterial toxins and particulate matter. *Immunity* **38**, 1142-1153 (2013).
9. R. Schreiber, F. Zhang, D. Haussinger, Regulation of vesicular pH in liver macrophages and parenchymal cells by ammonia and anisotonicity as assessed by fluorescein isothiocyanate-dextran fluorescence. *Biochem J* **315 (Pt 2)**, 385-392 (1996).
10. C. J. Gross *et al.*, K(+) Efflux-Independent NLRP3 Inflammasome Activation by Small Molecules Targeting Mitochondria. *Immunity* **45**, 761-773 (2016).
11. L. Luo, R. M. Lucas, L. Liu, J. L. Stow, Signalling, sorting and scaffolding adaptors for Toll-like receptors. *J Cell Sci* **133**, jcs239194 (2019).
12. S. Mariathasan *et al.*, Cryopyrin activates the inflammasome in response to toxins and ATP. *Nature* **440**, 228-232 (2006).
13. V. Hornung *et al.*, Silica crystals and aluminum salts activate the NALP3 inflammasome through phagosomal destabilization. *Nat Immunol* **9**, 847-856 (2008).
14. S. H. Chang *et al.*, Imiquimod Accelerated Antitumor Response by Targeting Lysosome Adaptation in Skin Cancer Cells. *J Invest Dermatol* **141**, 2219-2228 e2218 (2021).
15. E. E. To *et al.*, Endosomal NOX2 oxidase exacerbates virus pathogenicity and is a target for antiviral therapy. *Nat Commun* **8**, 69 (2017).
16. J. Thyberg, S. Moskalewski, Microtubules and the organization of the Golgi complex. *Exp Cell Res* **159**, 1-16 (1985).
17. I. Diaz-Del-Olmo *et al.*, Internalization of the Membrane Attack Complex Triggers NLRP3 Inflammasome Activation and IL-1beta Secretion in Human Macrophages. *Front Immunol* **12**, 720655 (2021).
18. F. Mallard *et al.*, Direct pathway from early/recycling endosomes to the Golgi apparatus revealed through the study of shiga toxin B-fragment transport. *J Cell Biol* **143**, 973-990 (1998).
19. F. R. Maxfield, T. E. McGraw, Endocytic recycling. *Nat Rev Mol Cell Biol* **5**, 121-132 (2004).
20. B. D. Grant, J. G. Donaldson, Pathways and mechanisms of endocytic recycling. *Nat Rev Mol Cell Biol* **10**, 597-608 (2009).
21. C. J. Noakes, G. Lee, M. Lowe, The PH domain proteins IPIP27A and B link OCRL1 to receptor recycling in the endocytic pathway. *Mol Biol Cell* **22**, 606-623 (2011).
22. C. Liang *et al.*, Beclin1-binding UVRAG targets the class C Vps complex to coordinate autophagosome maturation and endocytic trafficking. *Nat Cell Biol* **10**, 776-787 (2008).

23. J. P. Green *et al.*, Chloride regulates dynamic NLRP3-dependent ASC oligomerization and inflammasome priming. *Proc Natl Acad Sci U S A* **115**, E9371-E9380 (2018).
24. M. J. Daniels *et al.*, Fenamate NSAIDs inhibit the NLRP3 inflammasome and protect against Alzheimer's disease in rodent models. *Nat Commun* **7**, 12504 (2016).
25. B. Stechmann *et al.*, Inhibition of retrograde transport protects mice from lethal ricin challenge. *Cell* **141**, 231-242 (2010).
26. Z. Zhang *et al.*, Distinct changes in endosomal composition promote NLRP3 inflammasome activation. *Nat Immunol*, doi: 10.1038/s41590-022-01355-3 (2022).
27. L. Andreeva *et al.*, NLRP3 cages revealed by full-length mouse NLRP3 structure control pathway activation. *Cell* **184**, 6299-6312 e6222 (2021).
28. G. R. Hammond, M. P. Machner, T. Balla, A novel probe for phosphatidylinositol 4-phosphate reveals multiple pools beyond the Golgi. *J Cell Biol* **205**, 113-126 (2014).
29. C. B. Xie *et al.*, Complement Membrane Attack Complexes Assemble NLRP3 Inflammasomes Triggering IL-1 Activation of IFN-gamma-Primed Human Endothelium. *Circ Res* **124**, 1747-1759 (2019).
30. A. Baroja-Mazo *et al.*, Early endosome autoantigen 1 regulates IL-1beta release upon caspase-1 activation independently of gasdermin D membrane permeabilization. *Sci Rep* **9**, 5788 (2019).
31. S. Arumugam *et al.*, GSK3beta mediates the spatiotemporal dynamics of NLRP3 inflammasome activation. *Cell Death Differ* **29,** 2060–2069 (2022).

Acknowledgments

We are grateful to Professor Philip Woodman of the University of Manchester for useful advice and guidance on endosome trafficking assays and to the Bioimaging and Flow Cytometry Core Facilities.

Funding

We are grateful to the following funding agencies for funding this research: The Medical Research Council (MRC, UK) grant MR/T016515/1 (DB, ML), Wellcome Trust and Royal Society Henry Dale Fellowship 104192/Z/14/Z (GLC), and British Heart Foundation Accelerator Award AA/18/4/34221 to The University of Manchester (DB, RW). For the purpose of open access, the author has applied a Creative Commons Attribution (CC BY) license to any Author Accepted Manuscript version arising.

Author contributions

Author contributions are as follows:

Conceptualization: DMW, ML, DB, GLC

Methodology: AA, HB, GLC,

Investigation: BL, DMW, FMS, RW, CH, PIS, JPG, BJM

Visualization: BL, FMS, RW, CH, PIS, JPG, DB, ML, GLC

Funding acquisition: DB, ML, GLC

Project administration: DB, ML, GLC

Supervision: DB, ML, GLC

Writing – original draft: DB, ML, GLC

Writing – review & editing: DB, ML, GLC, BL, JPG, CH, PIS, RW,

Competing interests

The authors declare that they have no competing interests.

Data and materials availability

All data needed to evaluate the conclusions in the paper are present in the paper or the Supplementary Materials. Plasmids and cell lines are available from D.B. and M.P.L. under a material transfer agreement with the University of Manchester.

Figure Legends

Fig. 1. TGN46 co-localizes with endolysosomal membrane markers in COS7 cells treated with NLRP3-activating stimuli. **(A)** Representative immunofluorescence images of TGN46 and Golgin97 in COS7 cells stimulated for 90 min with vehicle (Veh, 0.5% ethanol (v/v)), nigericin (Nig, 10 µM), or monensin (Mon, 10 µM). See fig. S1A-C for images of COS7 cells stimulated with LLOMe (LL, 1 mM) and imiquimod (IQ, 75 µM). **(B)** Quantification of stimulus-induced colocalization of TGN46 and Golgin97 with the Pearson's correlation coefficient (PCC). Data are n=45 cells per group from 3 independent experiments (15 cells per experiment). **(C)** Representative immunofluorescence images of TGN46 and EEA1 in COS7 cells stimulated with vehicle, nigericin or monensin. See fig. S1A-C for images of COS7 cells stimulated with LLOMe and imiquimod. **(D)** Quantification of stimulus-induced colocalization of TGN46 and EEA1 with the Pearson's correlation coefficient (PCC). Data are n=45 cells per group from 3 independent experiments (15 cells per experiment). **(E)** Representative immunofluorescence images of TGN46 and CD63 in COS7 cells stimulated with vehicle, nigericin or monensin. See fig. S1A-C for images of COS7 cells stimulated with LLOMe and imiquimod. **(F)** Quantification of stimulus-induced colocalization of TGN46 and CD63 with the Pearson's correlation coefficient (PCC). Data are n=15 random fields of view per group from 3 independent experiments (5 fields of view per experiment). Blue represents nuclei staining by DAPI. Yellow arrows indicate co-localization at the Golgi. White arrows indicate co-localization on puncta. Scale bars: 10 µm. Values are median ± interquartile range (IQR). Data were analyzed using Kruskal-Wallis test followed by Dunn's multiple comparison test (compared to vehicle) (B, D) or one-way ANOVA followed by Dunnett's multiple comparison test (compared to vehicle) (F).*, $P \leq 0.05$; ***, $P \leq 0.001$.

Fig. 2. TGN38 co-localizes with EEA1 in BMDMs treated with NLRP3-activating stimuli. BMDMs were primed for 4 h with LPS (1 µg mL^{-1}), with the exception of vehicle. To prevent NLRP3-dependent cell death, MCC950 (10 µM) was applied 15 min before stimulation. **(A)** Representative immunofluorescence images of TGN38 and Golgin97 in BMDMs stimulated for 90 min with vehicle (Veh, 0.5% ethanol (v/v)), nigericin (Nig, 10 µM), or monensin (Mon, 10 µM). See also fig. S6A for images of BMDMs stimulated with LLOMe (LL, 1 mM) or imiquimod (IQ, 75 µM). **(B)** Quantification of stimulus-induced colocalization of TGN38 and Golgin97 with the Pearson's correlation coefficient (PCC). Data are n=9 (except LPS alone where n=8) random fields of view per group from 3 independent experiments. **(C)** Representative immunofluorescence images of TGN38 and EEA1 in BMDMs stimulated with vehicle, nigericin

or monensin. See also fig. S6B for images of BMDMs stimulated with LLOMe or imiquimod. **(D)** Quantification of stimulus-induced colocalization of TGN38 and EEA1 with the Pearson's correlation coefficient (PCC). Data are n=9 random fields of view per group from 3 independent experiments. **(E)** IL-1β release in response to stimuli. n=3 independent experiments. Blue represents nuclei staining by DAPI. Yellow arrows indicate instances of co-localization at the Golgi. White arrows indicate co-localization on puncta. Scale bars: 10 μm. IL-1β release was measured by ELISA. Values are median ± IQR (B, D) or mean ± SEM (E). Data were analyzed using one-way ANOVA followed by Dunnett's multiple comparison test (compared to vehicle) (B) or Kruskal-Wallis test followed by Dunn's multiple comparison test (compared to vehicle) (D, E) .*, $P \leq 0.05$; ***, $P \leq 0.001$.

Fig. 3. Endosomal trafficking is disrupted by NLRP3-activating stimuli. (A) Shiga toxin B (STxB) is endocytosed and trafficked from the plasma membrane to the trans-Golgi network (TGN) through endosomes. **(B)** HeLa cells pretreated with vehicle (Veh), nigericin (Nig 10 μM), LLOMe (LL, 1 mM), imiquimod (IQ, 75 μM) or monensin (Mon, 10 μM) were incubated with STxB-Cy3 (0.4 μg mL^{-1}). Quantification of STxB-Cy3 trafficking to the TGN was measured by the change in Pearson's correlation coefficient (PCC) between STxB-Cy3 and Golgin97 at 20 and 45 min (compared to 0 min) following STxB-Cy3 addition (n = 20-24 random fields of view per group from 5 independent experiments). **(C)** Representative immunofluorescence images of STxB-Cy3 (cyan) and Golgin97 (red) in HeLa cells treated with vehicle, nigericin or monensin from (B). **(D)** Transferrin binds to the transferrin receptor and is endocytosed into early endosomes, where it releases bound iron, before cycling back to the plasma membrane to be released extracellularly. **(E)** HeLa cells were treated with transferrin-488 (5 μg mL^{-1}) and with either vehicle, nigericin, LLOMe, imiquimod, or monensin for 30 min before media containing unlabelled transferrin and the indicated stimulus was added. Quantification of remaining cell-associated transferrin-488 was measured by the fluorescence intensity of transferrin-488 at 15 and 30 min following removal of extracellular transferrin-488 (n = 97-117 cells per group from 3 fields of view from 4 independent experiments). **(F)** Representative immunofluorescence images of transferrin-488 (Tf, green) in HeLa cells treated with vehicle, nigericin or monensin from (E). **(G)** EGF binds to its receptor, which is endocytosed and trafficked through the endo-lysosomal pathway, resulting in degradation of EGF. **(H)** HeLa cells were incubated with EGF-488 (0.4 μg mL^{-1}) on ice for 1 h (to allow surface binding of EGF-488) before extracellular EGF-488 was removed and cells were treated with vehicle, nigericin, LLOMe, imiquimod or monensin at 37ºC.

Quantification of EGF-488 degradation was measured by the fluorescence intensity of EGF-488 at 1 and 2 h following incubation at 37ºC (n=75-95 cells per group from 3 random fields of view from 4 independent experiments). **(I)** Representative immunofluorescence images of EGF-488 (green) in HeLa cells treated with vehicle, nigericin or monensin from (G). Scale bars: 10 µm. Values are median ± IQR. Data were analyzed using Kruskal-Wallis test followed by Dunn's multiple comparison test (compared to vehicle for each time point) (B, E&H). *, P≤0.05; **, P≤ 0.01; ***, P≤ 0.001.

Fig. 4. Monensin potentiates imiquimod-induced NLRP3 activation in primary and immortalized BMDMs. (A-D) LPS-primed primary BMDMs were treated with vehicle or monensin (Mon, 10 µM) for 2 h before being stimulated with imiquimod (IQ, 75 µM) for 2 h. Supernatants were assessed for IL-1β (measured by ELISA) (A) and LDH (B) release (n = 4 independent experiments). Cell lysates and supernatants were assessed for DSS-crosslinked ASC oligomers (C) (n = 3 independent experiments) or inflammatory protein content by Western blotting (D) (n = 4 independent experiments). **(E-F)** LPS-primed primary BMDMs were treated with vehicle or monensin (10 µM) for 2 h prior to MCC950 treatment (10 µM, 15 min) before being stimulated with imiquimod (75 µM) for 2 h. Supernatants were assessed for IL-1β (E) and LDH (F) release (n = 4 independent experiments). **(G-H)** LPS-primed WT iBMDMs were treated with vehicle or monensin (10 µM) for 1 h before being stimulated with imiquimod (75 µM) for 2 h. Supernatants were assessed for IL-1β (G) and LDH (H) release (n = 6 independent experiments). **(I-L)** LPS-primed iBMDMs stably expressing ASC-mCherry were treated with vehicle or monensin (10 µM) for 2 h before being treated with Ac-YVAD-CMK (100 µM) for 15 min and stimulated with imiquimod (75 µM) for 2 h. ASC speck formation was measured (I), and ASC speck number at the final time point of 2 h is shown (J) (% of veh + imiquimod treatment) (n = 6 independent experiments). Number of cells containing an ASC speck at 2 h (K) and mean number of ASC specks per speck-positive cell were counted (L). **(M)** LPS-primed iBMDMs were treated with vehicle or monensin (10 µM) for 1 h before being stimulated with imiquimod (75 µM) for 2 h. Cell lysates and supernatants were assessed for DSS-crosslinked ASC oligomers (n = 4 independent experiments). Values are mean ± SEM. Data were analyzed using unpaired two-tailed Mann-Whitney test (Veh+IQ compared to Mon+IQ) (A, B, G, H, K), Kruskal-Wallis test followed by Dunn's multiple comparison test (Veh+Veh+IQ compared to Veh+MCC950+IQ, Mon+Veh+IQ compared to Mon+MCC950+IQ) (E, F), or multiple unpaired Mann-Whitney tests compared to a value of 100% followed by Holm-Sidak correction (J). *, P≤0.05; **, P≤0.01.

Fig. 5. NLRP3-mVenus co-localizes with puncta positive for TGN46, EEA1, CD63, and LAMP1 in COS7 cells treated with NLRP3-activating stimuli. (A-C) Immunofluorescence images of COS7 cells stably expressing NLRP3-mVenus and stimulated for 90 min with vehicle (0.5% ethanol (v/v)), nigericin (10 µM) or monensin (10 µM). Line graphs depicting changes in fluorescence intensity (min = 0, max = 250) over 10 µm for each stimulus and stain are shown. Images are representative of 3 independent experiments. Blue represents nuclei staining by DAPI. White arrows indicate co-localization between NLRP3 and puncta positive for EEA1 (A), CD63 (B), or LAMP1 (C). Yellow arrows indicate NLRP3 puncta alone. Dashed lines highlight the areas depicted in the magnified insets. Scale bars: 10 µm.

Fig. 6. NLRP3-mVenus co-localizes with PI4P on CD63- and LAMP1-positive puncta in COS7 cells treated with NLRP3-activating stimuli. (A, D, & F) Fluorescence and immunofluorescence images of COS7 cells stably expressing NLRP3-mVenus and stimulated for 90 min with vehicle (Veh, 0.5% ethanol (v/v)), nigericin (Nig, 10 µM) or monensin (Mon, 10 µM). Co-localization between NLRP3-mVenus, a reporter for PI4P (PI4P) and Golgin97 (A), CD63 (D), or LAMP1 (F) was assessed. Line graphs depicting changes in fluorescence intensity (min = 0, max = 250) over 10 µm for each stimulus and stain are shown. White arrows indicate co-localization between NLRP3, PI4P, and puncta positive for CD63 (D), or LAMP1 (F). Blue arrow indicates co-localization between NLRP3 and PI4P alone. Yellow arrow indicates NLRP3 puncta alone. Images are representative of 3 (A&F) and 4 (D) independent experiments. Blue represents nuclei staining by DAPI. Dashed lines highlight the areas depicted in the zoomed insets. Scale bars: 10 µm. **(B)** Quantification of stimulus-induced colocalization of PI4P and NLRP3 with the Pearson's correlation coefficient (PCC) (n=12-15 cells per group from 3 random fields of view from 3 independent experiments). **(C)** Quantification of stimulus-induced colocalization of PI4P and Golgin97 with the Pearson's correlation coefficient (PCC) (n=18-20 cells per group from 3 random fields of view from 3 independent experiments). **(E)** Quantification of stimulus-induced colocalization of PI4P and CD63 with the Pearson's correlation coefficient (PCC) (n=17-20 cells per group from 3 random fields of view from 4 independent experiments). **(G)** Quantification of stimulus-induced colocalization of PI4P and LAMP1 with the Pearson's correlation coefficient (PCC) (n=15-22 cells per group from 3 random fields of view from 3 independent experiments).

Values are median ± IQR. Data were analyzed using one-way ANOVA followed by Dunnett's multiple comparison test (compared to vehicle) (B, C, E, G). *, P≤0.05; ***, P≤ 0.001.

Fig. 7. Diagram summarizing the importance of endosomal trafficking proposed in this study. (**A** to **C**) TGN38/46 cycles between the TGN and plasma membrane through endosomes (A). NLRP3 inflammasome-activating stimuli cause a disruption of endolysosomal trafficking (B) resulting in the production of PI4P and recruitment of NLRP3 (C).

Fig 1

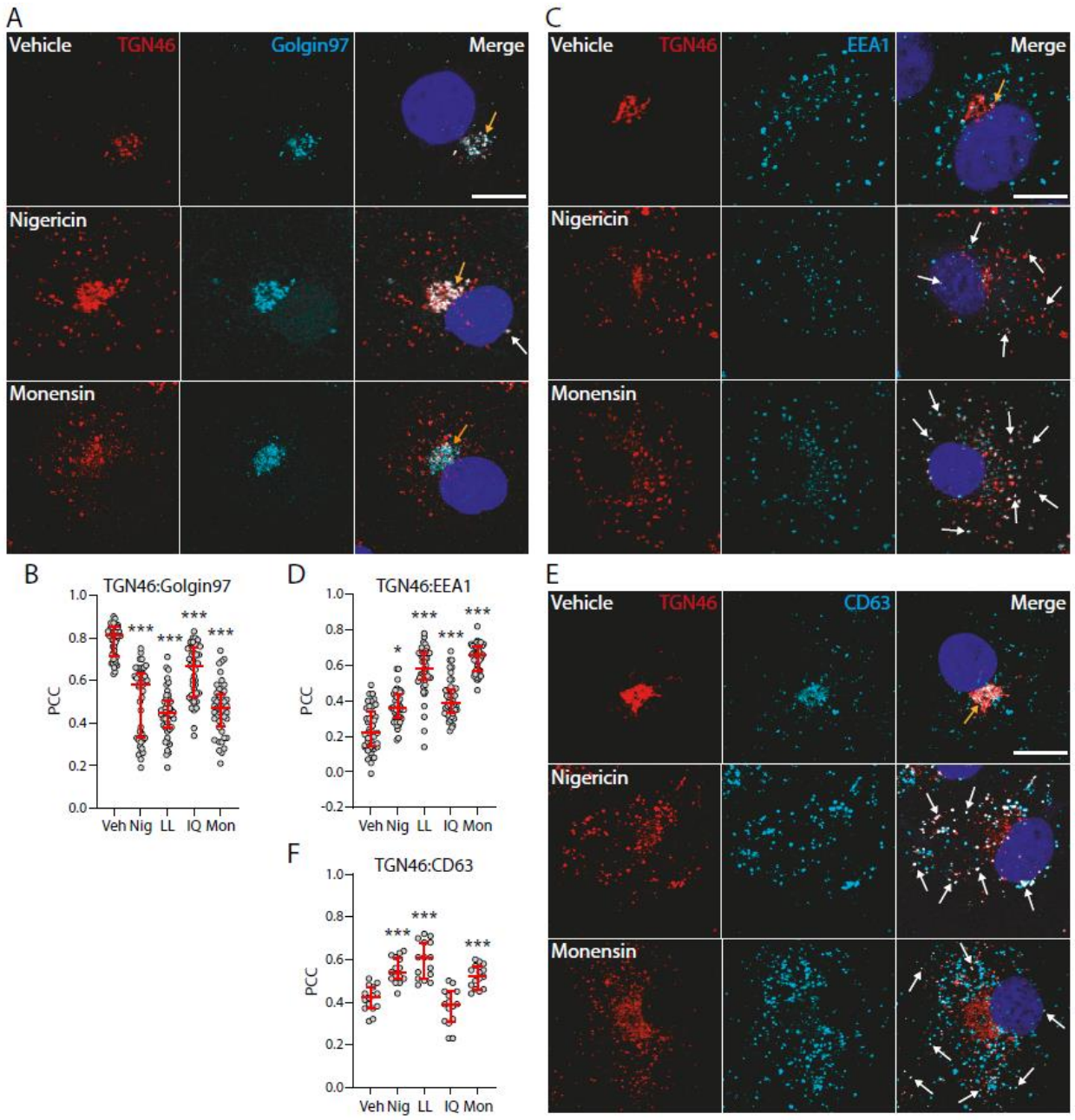
A
Vehicle
TGN46
Golgin97
Merge
Nigericin
Monensin
C
Vehicle
TGN46
EEA1
Merge
Nigericin
Monensin
B
TGN46:Golgin97
PCC
Veh Nig LL IQ Mon
D
TGN46:EEA1
PCC
Veh Nig LL IQ Mon
E
Vehicle
TGN46
CD63
Merge
Nigericin
Monensin
F
TGN46:CD63
PCC
Veh Nig LL IQ Mon

Fig 2

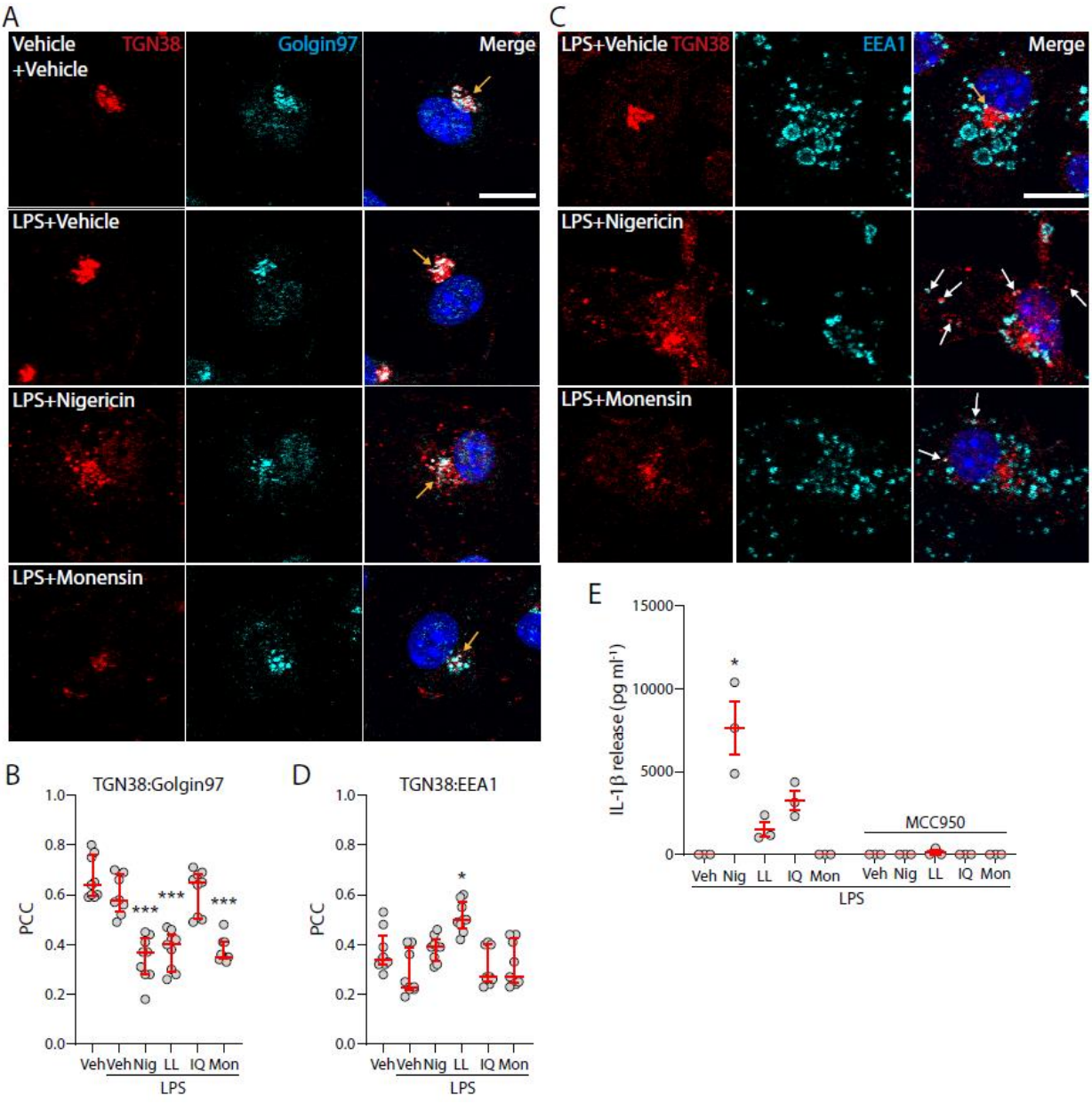
A
Vehicle +Vehicle
TGN38
Golgin97
Merge
LPS+Vehicle
LPS+Nigericin
LPS+Monensin
C
LPS+Vehicle
TGN38
EEA1
Merge
LPS+Nigericin
LPS+Monensin
B
TGN38:Golgin97
PCC
1.0
0.8
0.6
0.4
0.2
0.0
***
***
***
Veh Veh Nig LL IQ Mon
LPS
D
TGN38:EEA1
PCC
1.0
0.8
0.6
0.4
0.2
0.0
*
Veh Veh Nig LL IQ Mon
LPS
E
IL-1β release (pg ml-1)
15000
10000
5000
0
*
MCC950
Veh Nig LL IQ Mon Veh Nig LL IQ Mon
LPS

Fig 3

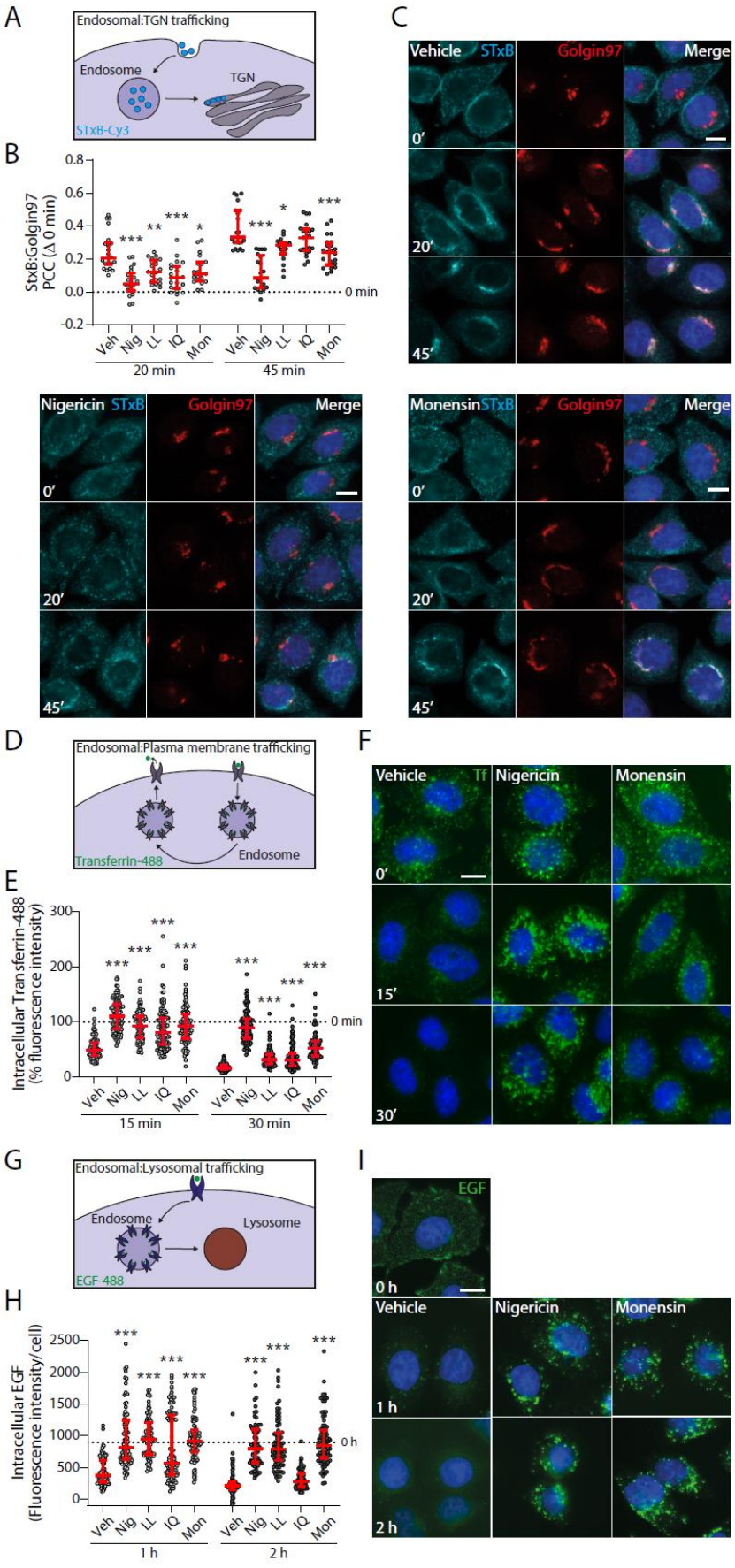
A
Endosomal:TGN trafficking
Endosome
TGN
STxB-Cy3
B
StxB:Golgin97 PCC (Δ 0 min)
0 min
Veh Nig LL IQ Mon
20 min
45 min
C
Vehicle STxB
Golgin97
Merge
0′
20′
45′
Nigericin STxB
Monensin STxB
D
Endosomal:Plasma membrane trafficking
Transferrin-488
Endosome
E
Intracellular Transferrin-488 (% fluorescence intensity)
15 min
30 min
F
Vehicle Tf
Nigericin
Monensin
15′
30′
G
Endosomal:Lysosomal trafficking
Endosome
Lysosome
EGF-488
H
Intracellular EGF (Fluorescence intensity/cell)
0 h
1 h
2 h
I
EGF

Fig 4

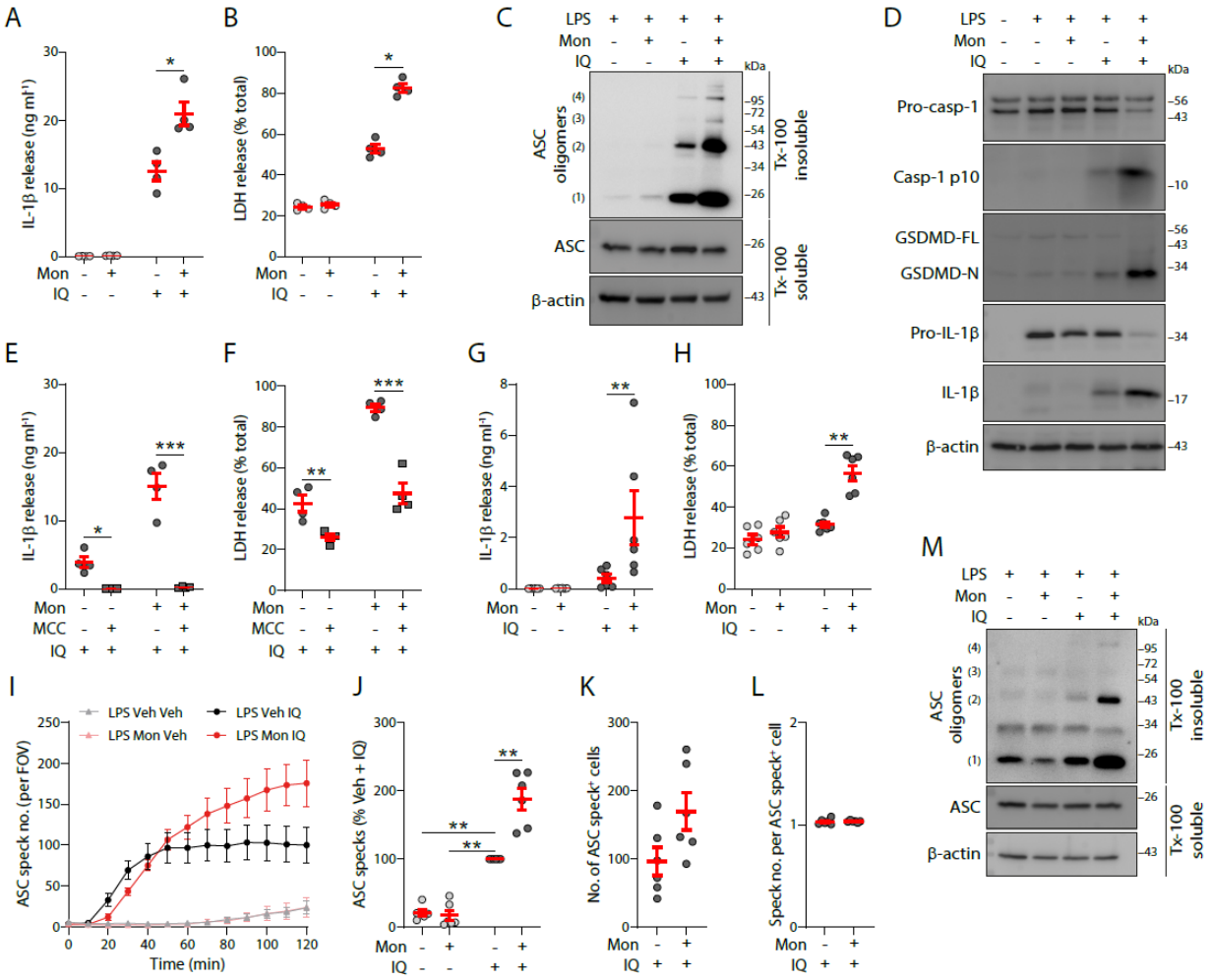
A
B
C
D
E
F
G
H
I
J
K
L
M
IL-1β release (ng ml⁻¹)
LDH release (% total)
Mon
IQ
MCC
LPS
kDa
ASC oligomers
Tx-100 insoluble
ASC
Tx-100 soluble
β-actin
Pro-casp-1
Casp-1 p10
GSDMD-FL
GSDMD-N
Pro-IL-1β
IL-1β
LPS Veh Veh
LPS Mon Veh
LPS Veh IQ
LPS Mon IQ
ASC speck no. (per FOV)
Time (min)
ASC specks (% Veh + IQ)
No. of ASC speck⁺ cells
Speck no. per ASC speck⁺ cell

Fig 5

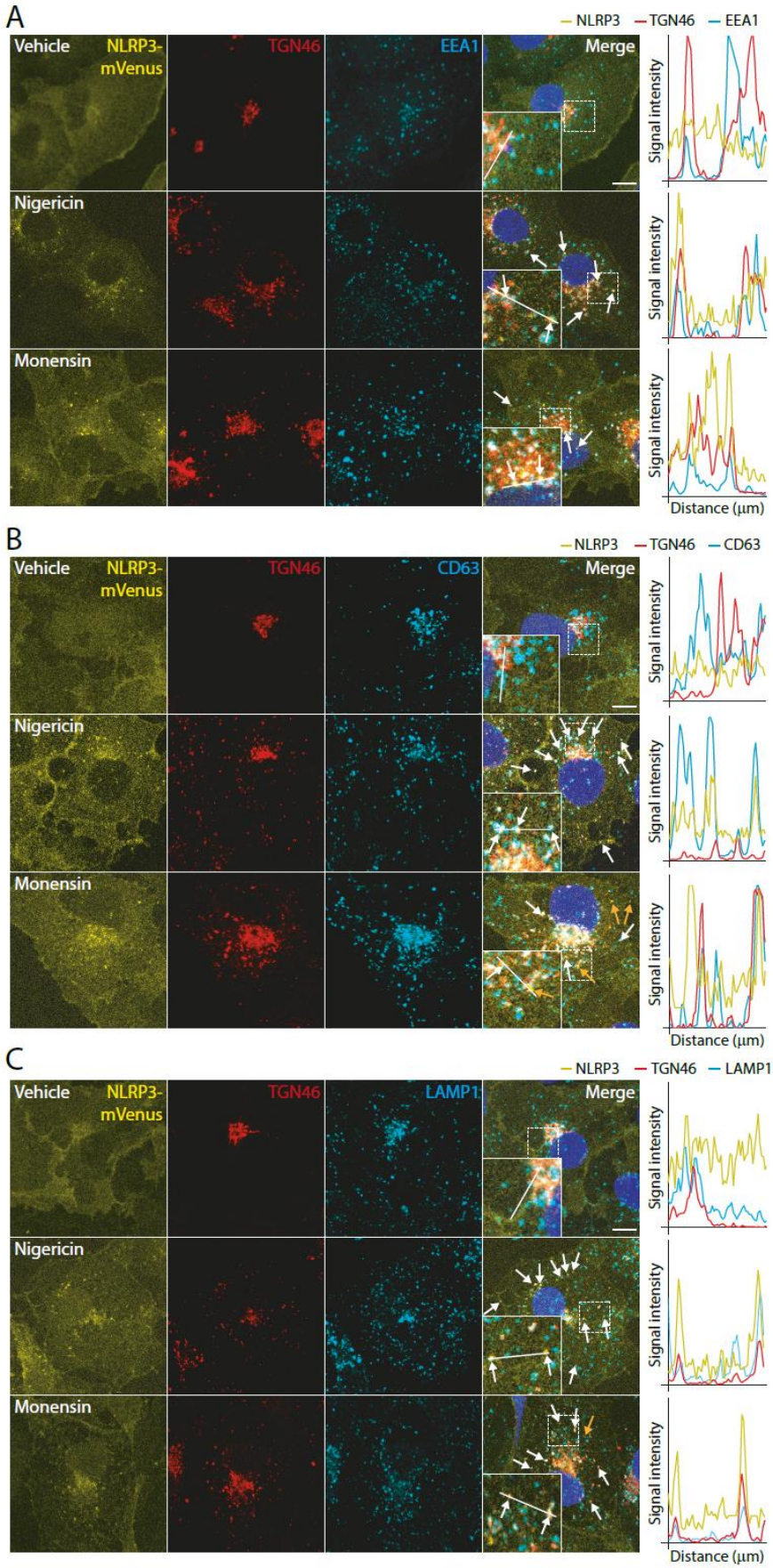
A
NLRP3
TGN46
EEA1
Vehicle
NLRP3-mVenus
TGN46
EEA1
Merge
Nigericin
Monensin
Signal intensity
Distance (μm)
B
NLRP3
TGN46
CD63
Vehicle
NLRP3-mVenus
TGN46
CD63
Merge
Nigericin
Monensin
Signal intensity
Distance (μm)
C
NLRP3
TGN46
LAMP1
Vehicle
NLRP3-mVenus
TGN46
LAMP1
Merge
Nigericin
Monensin
Signal intensity
Distance (μm)

Fig 6

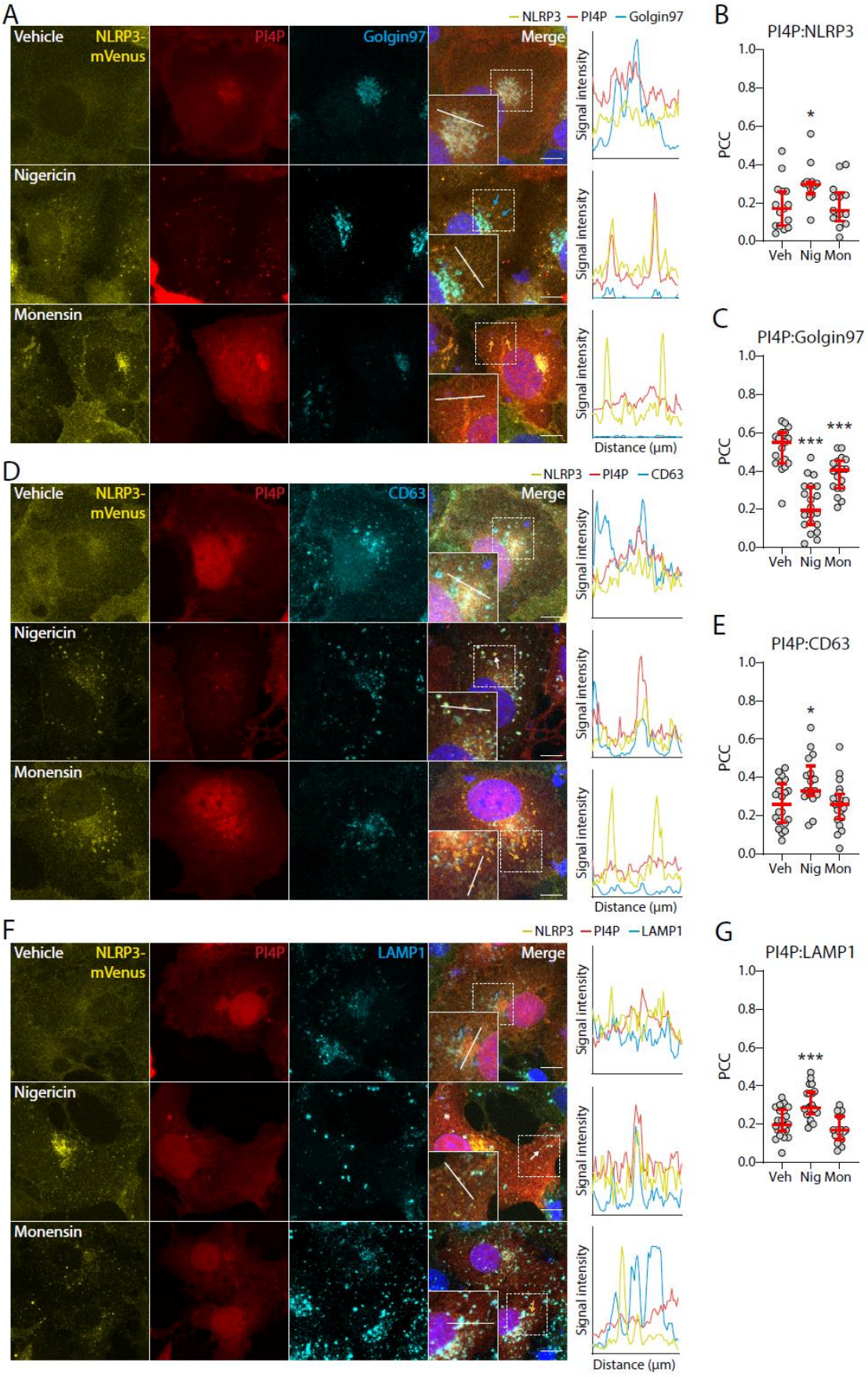
A
Vehicle
NLRP3-mVenus
PI4P
Golgin97
Merge
NLRP3 PI4P Golgin97
Nigericin
Monensin
Signal intensity
Distance (μm)
B
PI4P:NLRP3
PCC
Veh Nig Mon
C
PI4P:Golgin97
D
CD63
NLRP3 PI4P CD63
E
PI4P:CD63
F
LAMP1
NLRP3 PI4P LAMP1
G
PI4P:LAMP1

Fig 7

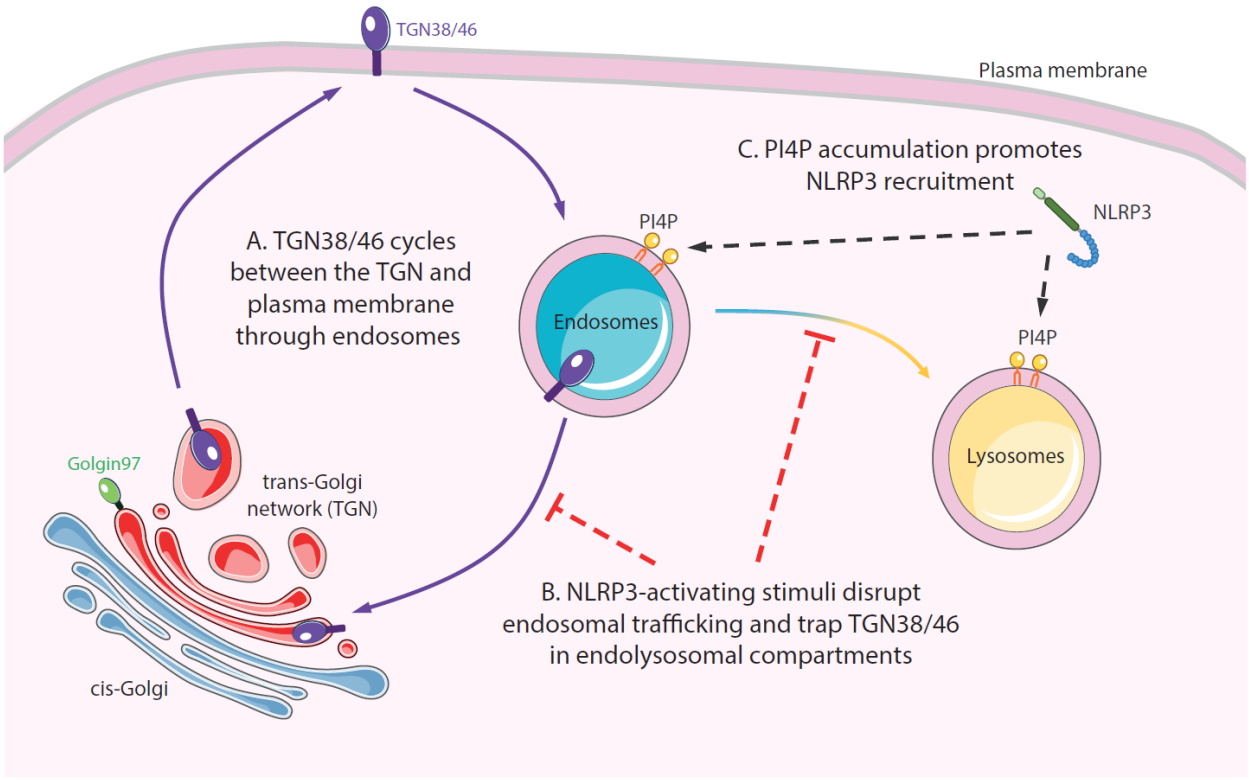
TGN38/46
Plasma membrane
C. PI4P accumulation promotes
NLRP3 recruitment
NLRP3
PI4P
A. TGN38/46 cycles
between the TGN and
plasma membrane
through endosomes
Endosomes
PI4P
Lysosomes
Golgin97
trans-Golgi
network (TGN)
cis-Golgi
B. NLRP3-activating stimuli disrupt
endosomal trafficking and trap TGN38/46
in endolysosomal compartments